ACS OMEGA

Open Access

http://pubs.acs.org/journal/acsodf

Article

Lignin-Based Nanospheres as Environmental Remediation Platforms for Anionic Dye Contaminants

Fei Zhang, Ha Na, Jake Carrier, Chen-Yu Chang, Daniela Radu, and Cheng-Yu Lai*

Cite This: *ACS Omega* 2024, 9, 12006−12014

Read Online

ACCESS | Metrics & More | Article Recommendations | Supporting Information

ABSTRACT: Modern manufacturing of textiles, pharmaceuticals, food, cosmetics, plastics, paper, etc. involves the utilization of anionic and cationic dyes that lead to significant water contamination. Recent research has explored the use of nanomaterials toward developing nanoadsorbents for water decontamination caused by industrial pollution. Here, we report on a novel platform for anionic dye remediation, consisting of a polyethylenimine-functionalized lignin nanosphere (PEI-LNS). The designed nanomaterial shows significant ability to adsorb an anionic dye selected as a proof-of-concept—Sulforhodamine B, from aqueous solutions. The PEI lignin nanoadsorbents (PEI-LNS) showed a better ability to adsorb Sulforhodamine B sodium salt (SBSS) when compared to the raw lignin nanosphere adsorbent (LNS), especially in acidic conditions. The nanomaterial was characterized through transmission electron microscopy, scanning electron microscopy, Brunauer−Emmett−Teller surface area analysis, elemental analysis, zeta potential, thermogravimetric analysis, Fourier transform infrared spectroscopy, and nuclear magnetic resonance. The impacts of ionic strength, contact time, pH, and adsorbent concentration have been evaluated. The ability of PEI-LNS to adsorb SBSS was found to be consistent with Langmuir isotherms and pseudo-second-order kinetic models. The PEI-LNS could be recycled three times, reaching a good (85%) adsorbing capacity even in the third cycle. The study demonstrates that PEI-LNS has a strong affinity as a novel adsorbent for anionic dyes and could be employed in environmental cleanups pertaining to such contaminations.

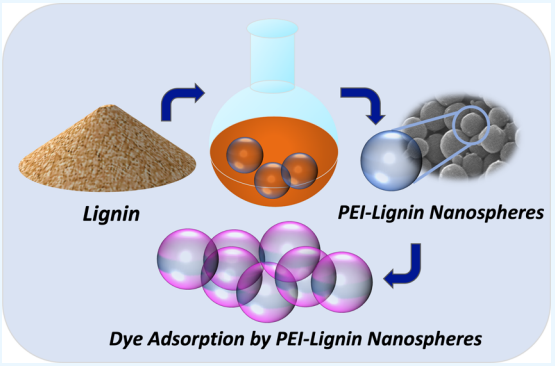

1. INTRODUCTION

Access to clean water is vital to the ecosystem's survival. However, global industrialization along with population growth drove increased water pollution, demanding fast and inexpensive remediation solutions. Among such pollutants, anionic dyes are significant water contaminants due to their known toxicity to many living organisms.[1] Dyes and pigments used for dyeing and printing natural, synthetic, man-made, and mixed textile materials, such as wool, silk, nylon, polyester, acrylics, polyacetate, and polyurethane, can reach 100,000 types on the market, of which world annual production is about 700,000 tones.[2] Various techniques to remediate pollution resulting from wastewater containing dyes, including oxidative degradation, photodegradation, electrocoagulation, and biochemical degradation, have been explored over the years, but they lack scalability. In contrast, adsorption is a scalable and reliable technique for dye and other organic contaminants removal. The method is inexpensive, easy to implement, and displays high efficiency in eliminating the contaminants.[3] The fabricated adsorbents could be engineered to eliminate dyes from concentrated solutions and to be recycled through regeneration.[4,5] Adsorbents based on nanomaterials, including carbon nanotubes, graphene sheets, and metal oxides, have received an increased attention for the treatment of water and wastewaters provided their strong adsorption affinities for various organic compounds.[6] However, these are not cost-effective. In this line, biorenewable materials, especially of lignocellulosic origin, are appealing platforms for producing sorbent materials, toward development of inexpensive and environmentally friendly treatment methods necessary to adequately treat dye-containing wastewater prior to being discharged into the environment.[7]

As one of the main components of all vascular plants, lignin is the second most abundant natural biopolymer material, representing 25% of all nonfossil organic carbon on Earth, and it is largely unutilized; its availability exceeds 300 billion tons.[8−11] Lignin is a three-dimensional biopolymer coexisting with hemicellulose and cellulose in plants.[12−16] Structurally, lignin is a complex polymer network of various organic functional groups,[17] and it has been functionalized through various pathways, such as amination, sulfonation, esterification, and copolymerization, for a plethora of applications.[18]

Received: December 8, 2023
Revised: February 20, 2024
Accepted: February 21, 2024
Published: March 1, 2024

Recently, modified lignin has been reported as an effective adsorbent of organics (e.g., methylene blue, Procion Blue, and phenols), metals (e.g., Cu, Zn, Pb, and Pt), volatile organic compounds (VOCs), ammonia (NH_3), and sulfur dioxide (SO_2).[17]

This study focuses on investigating the feasibility of lignin as a platform for the fabrication of organic dye adsorbents. To enhance reproducibility of this process and the enhanced accessible aminated surface area, this work employed uniform-sized nanospheres, reporting on the first polyaminated lignin nanosphere (LNS) for environmental remediation. Removal of anionic dyes is favored at pH 2−4, and therefore, in this acidic pH range, the adsorbent surface should be positively charged to adequately adsorb negatively charged anionic dyes.[19] We report the preparation and proof-of-concept validation of polyamine-functionalized lignin spherical particles with the capability to remove anionic contaminants from water waste streams. To increase the accessible surface area of the sorbent, lignin was processed to render spherical particles with a narrow particle size distribution in the vicinity of 220 nm. Upon synthesis, the LNSs were further functionalized with polyethylenimine (PEI) using a silane linker. As a proof-of-concept of effective anionic dye remediation, we utilized Sulforhodamine B sodium salt (SBSS)—an anionic dye belonging to the family of fluorescent rhodamine water-soluble organic dyes and selected for its fluorescent properties, which enables imaging of sorbent postadsorption. The results demonstrate that the novel lignin-amine platform efficiently removes SBSS from water under acidic conditions.

2. EXPERIMENTAL SECTION

2.1. Materials. The lignin particles used in this work were prepared from a commercial softwood kraft lignin, courtesy sample (Indulin AT) supplied by Ingevity, Inc. (North Charleston, SC), and used without further purification. Trimethoxysilylpropyl-modified polyethylenimine (TMS-PEI) (Gelest, M_w: 1500−1800 g/mol, 50% in isopropanol), sodium hydroxide (NaOH), sodium chloride (NaCl), hydrochloric acid (HCl), acetone, and SBSS were purchased from Thermo Fisher Scientific (Waltham, MA, USA).

2.2. Preparation of LNS. First, Indulin AT kraft lignin (200 mg) was dissolved in a 40 mL acetone aqueous solution (3:1 acetone and nanopure water, v: v), and the mixture was magnetically stirred overnight at room temperature followed by a 15 min ultrasonication. Next, the insoluble residues were removed by centrifugation at 2500 rpm for 15 min. The supernatant was transferred to a round-bottom flask (100 mL) and acetone was removed by a rotary evaporator (40 °C, 150 rpm). The resulting LNSs were redispersed/washed in nanopure water and collected via centrifugation (8000 rpm, 15 min) followed by drying in a vacuum oven overnight at room temperature.

2.3. Formation Mechanism of LNS. The formation of LNS is attributed to the amphiphilic nature of lignin, which contains both hydrophobic and hydrophilic groups. Lignin tends to organize itself into spherical nanoparticles, thereby maximizing the surface area in contact with the nonsolvent phase (usually water).[20] In addition, the hydrophobic effect may be related to other noncovalent interactions, such as van der Waals forces and $\pi-\pi$ stacking interactions.[21]

2.4. Synthesis of the PEI-LNS. TMS-PEI, 50% in isopropanol, was used to functionalize lignin with PEI in one step via a grafting reaction that takes advantage of the intrinsic alcohol groups in lignin. LNSs (200 mg) were dispersed in 15 mL of 0.5, 1.0, 2.0, and 3.0 mM TMS-PEI aqueous solution, respectively, and stirred overnight at 70 °C under argon. The formed PEI-LNSs (PEI-LNS-1/2/3/4, respectively) were thoroughly washed 3 times with nanopure water to remove the unreacted PEI. Then the resulting PEI-LNSs were dried in a vacuum oven overnight at room temperature.

2.5. Morphology of LNS and PEI-LNS. The particle geometry and average particle size were determined by scanning electron microscopy (SEM) and transmission electron microscopy (TEM). The SEM images were imported in the Nanomeasurer software,[22] which was used to assess the average diameter of the nanospheres.

2.6. Dye Adsorption. SBSS aqueous solution (10 mM, 5.8 g/L) was prepared as the stock solution. Serial dilutions of the SBSS stock solution were prepared in concentrations ranging from 0 to 1 mM. Lignin particles were dispersed in deionized water at predetermined concentrations and sonicated for 30 min. All the tests were carried out in 5 mL tubes by mixing the dye solution with PEI-LNS or LNS (for control experiments). The vials containing the mixture of SBSS and lignin dispersion were placed on a shaker at room temperature and allowed to mix overnight. The particles were then separated by centrifugation, and the supernatant was subjected to UV−vis measurement. PEI-LNS and LNS were used to adsorb SBSS at different pH values, sorbent dosages, contact times, and initial concentrations. The final pH values of the solutions were as follows: 2.2, 3.0, 4.0, 5.0, 6.0, 7.0, and 8.0, adjusted using prepared solutions of 0.1 mM HCl and 0.5 mM NaOH. The sorbent dosage varied from 0 to 0.45 mg/mL, the contact time ranged from 5 min to 16 h, and the dye concentration varied from 0 to 10 mg/L.

2.7. Characterization Methods. LNS and PEI-LNS imaging was performed with JEOL/JSM-F100 Schottky field emission scanning electron microscopy (FE-SEM) and a ThermoFisher Talos/F200X scanning transmission electron microscope (STEM) to determine particle size and morphology. Solution ^{1}H NMR spectra were obtained using a Bruker 600 MHz spectrometer and the solid-state nuclear magnetic resonance (NMR) on a Bruker with Avance-NEO-600 console (Bruker Corporation, MA, USA). Zeta potential was measured on a Malvern Zetasizer Nano-ZS ZEN3600 instrument operated at room temperature. Specific surface area of the nanomaterials was determined with a Quantachrome NOVA-touch LX-2 surface area analyzer. Nitrogen adsorption−desorption isotherms were collected at 77.35 K using high-purity nitrogen as an adsorbate gas. All samples were degassed prior to analysis at 100 °C for 16 h to remove adsorbed moisture. Surface area of each sample was determined using the Brunauer−Emmett−Teller (BET) theory, and pore size distribution was determined using the DFT model. Thermogravimetric analysis (TGA) was carried out by using a SDT Q600 under nitrogen flow of 100 mL/min. Fourier transform infrared spectroscopy (FT-IR) was conducted on a Shimadzu/IRTracer-100 instrument to identify the LNS and PEI-LNS functional groups. Ultraviolet−visible (UV−vis) absorption spectroscopy was employed for producing the calibration curve of dye absorption using a UV−vis spectrophotometer (Thermo Scientific/BioMate 160). The pH of the working solutions was measured with a pH meter (Fisherbrand FE 150). All fluorescence microscopy imaging was performed by using an EVOS Fluorescence Imaging M7000 System (Thermo Fisher).

https://doi.org/10.1021/acsomega.3c09834
ACS Omega 2024, 9, 12006−12014

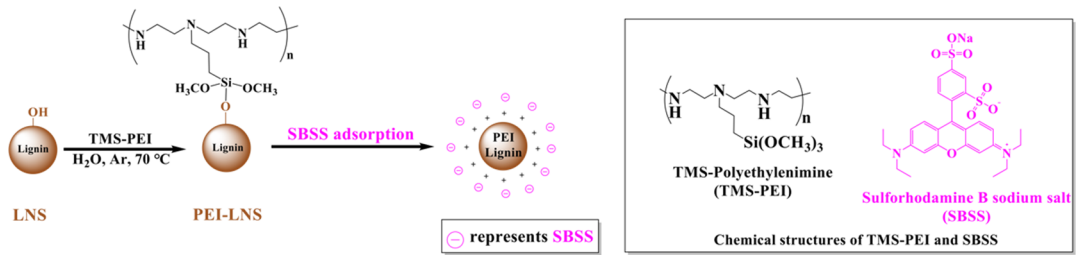

Figure 1. Schematic of PEI-LNS SBSS adsorption.

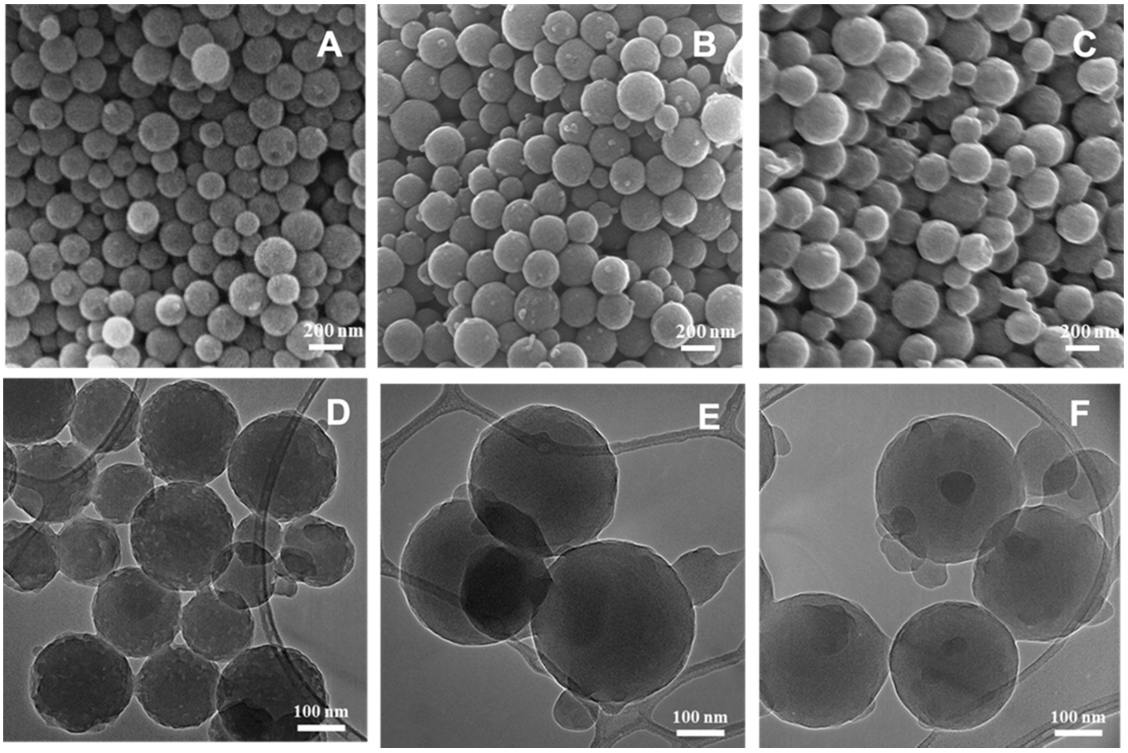

Figure 2. SEM and TEM characterization: FE-SEM of LNS (A), PEI-LNS (B), and PEI-LNS-2 after SBSS adsorption (C); and S/TEM images of LNS (D), PEI-LNS-2 (E), and PEI-LNS-2 after SBSS adsorption (F).

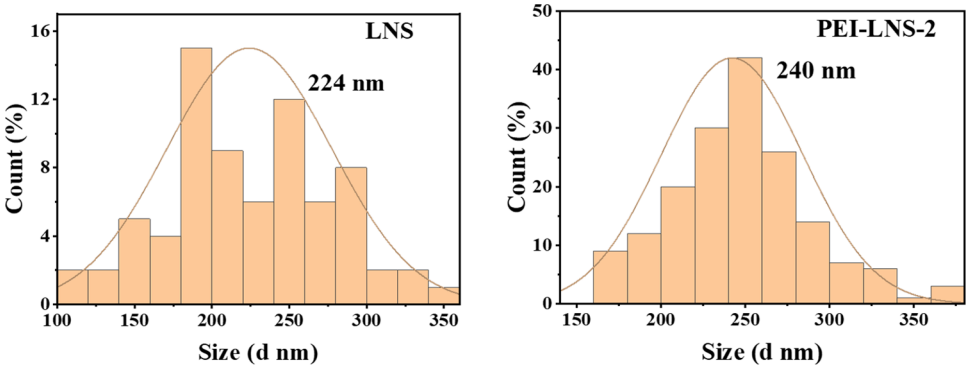

Figure 3. Estimate of particle size using SEM for LNS (left) and PEI-LNS-2 (right).

3. RESULTS AND DISCUSSION

We highlight herein the characteristics of the material that showed the highest adsorption capacity, PEI-LNS-2; the rest of the materials' characterization is available in the Supporting Information. Figure 1 shows a schematic representation of the sorbent fabrication and adsorption principle. In essence, in acidic conditions, the amine groups of the PEI-LNS are protonated, rendering the sorbent surface positively charged, and thus interacting noncovalently with the dye via electrostatic interactions.

3.1. Nanoparticle Size and Morphology. The morphology of LNS and PEI-LNS materials was determined by SEM and TEM (Figure 2 and Supporting Information, Figure S2). The LNS is a spherical structure with an average size of 224

https://doi.org/10.1021/acsomega.3c09834
ACS Omega 2024, 9, 12006−12014

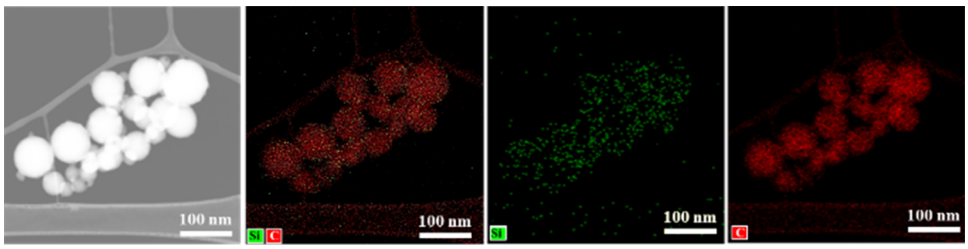

Figure 4. STEM EDX of PEI-LNS-2.

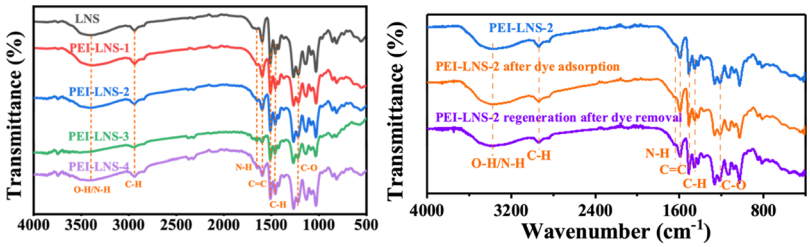

Figure 5. FT-IR analysis: LNS and PEI-LNS-1/2/3/4 (left); FT-IR spectra of the PEI-LNS, PEI-LNS-2 after SBSS adsorption, and PEI-LNS-2 regenerated after one cycle (right).

nm (Figure 3). After functionalization, the material selected for further investigation, PEI-LNS-2, showed an average diameter of 240 nm nanosphere (Figure 3), which is a slight increase in the average particle size and could be ascribed to the PEI layer.

3.2. Nanoparticle Compositional Analysis. *3.2.1. STEM EDX.* As supplementary evidence of the PEI layer, energy dispersive X-ray spectroscopy (EDX) performed concomitant with the STEM indirectly confirmed the presence of the PEI coverage through the presence of the silicon atoms on the surface of LNSs, given that Si is covalently linked to PEI (Figure 4).

3.2.2. FT-IR Analysis. FT-IR analysis was performed to investigate the presence of characteristic functional groups of lignin and amine and stability of the sorbent throughout the cycles (Figures 5, S8 and S9).[23,24] The peaks at 3400 cm^{-1} could be attributed to −OH/NH stretching, and the bands at approximately 2920 cm^{-1} are associated with C−H stretching in the methylene and methyl groups. In addition, the absorption peaks at 1600, 1512, and 1452 cm^{-1} were assigned to the −CH− vibration in aromatic rings.[25,26]

The trend and characteristic peaks of PEI-LNS are in good agreement with those of LNS, which indicates that the lignin structure remained intact after PEI grafting. The differences between the spectra are almost indistinguishable likely due to similarity in O−H stretching from amine, alcohols, acids, and phenols, all present in the PEI-LNS. The FT-IR of the postadsorption and regenerated samples also illustrates the significant similarity of the samples, which is indicative of good recyclability of the PEI-LNS sorbent.

3.2.3. NMR Spectroscopy. In contrast to FT-IR, both ^{1}H solution NMR solution and ^{13}C solid-state NMR show the distinguishable presence of ethylene groups in the amine proximity in the PEI-functionalized lignin (Supporting Information Figures S3 and S4).

3.2.4. Elemental Analysis. Elemental analysis enabled detection of the presence of nitrogen as direct evidence of PEI functionalization. As illustrated in Figure 6 and Table 1, the amount of nitrogen (mmol/g) in PEI-LSN matched the trend of the amount of TMS-PEI added during the synthesis.

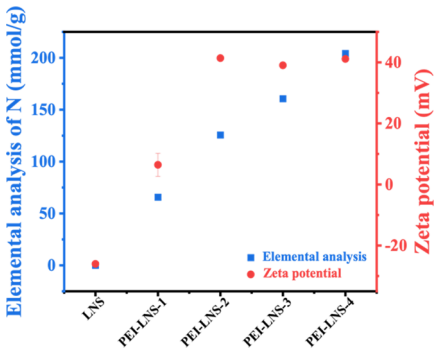

Figure 6. Results of elemental analysis and zeta potential of LNS and PEI-LNSs (1/2/3/4).

Table 1. Results of Elemental Analysis and Zeta Potential of LNS and PEI-LNS

sample	elemental analysis of N (mmol/g)	zeta potential (mV)
LNS	0	−26.03 ± 0.55
PEI-LNS-1	65.68	6.43 ± 3.78
PEI-LNS-2	125.65	41.1 ± 0.26
PEI-LNS-3	160.64	39.03 ± 0.58
PEI-LNS-4	204.19	41.13 ± 0.67

As anticipated, there is no nitrogen identified in the LNS samples.

3.2.5. Zeta Potential Analysis. The zeta potential analysis allows the determination of the surface charge. To identify the sorbent with the highest affinity for anionic contaminants in acidic waste streams, we measured the zeta potential of both LNS and PEI-functionalized LNS samples. By plotting both the nitrogen amount and zeta potential (Figure 6), we highlight the expected trend from positive charged particles LNS to increasing negative charged PEI-LNS as the nitrogen content corresponding to elevated amine density, increased.

3.2.6. Surface Area and TGA. The specific surface area of unmodified LNS, PEI-LNS, and PEI-LNS after SBSS adsorption and regeneration were determined from the nitrogen adsorption−desorption isotherms using the BET

https://doi.org/10.1021/acsomega.3c09834
ACS Omega 2024, 9, 12006−12014

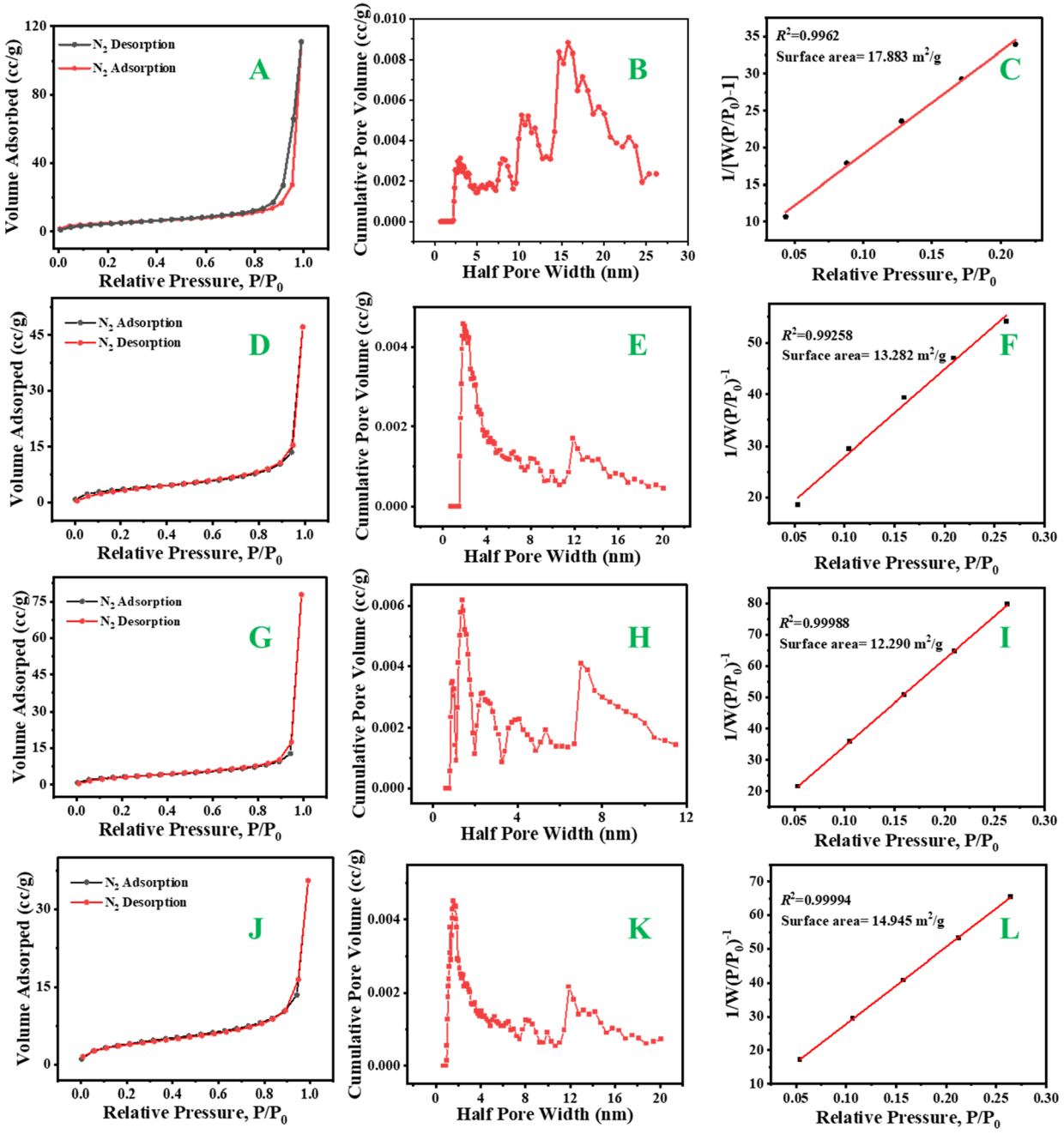

Figure 7. N_2 adsorption−desorption isotherm (A), DFT pore size distribution (B), and BET surface area distribution (C) of LNS; N_2 adsorption−desorption isotherm (D), DFT pore size distribution (E), and BET surface area distribution (F) of PEI-LNS-2; N_2 adsorption−desorption isotherm (G), DFT pore size distribution (H), and BET surface area distribution (I) of PEI-LNS-2 with SBSS; N_2 adsorption−desorption isotherm (J), DFT pore size distribution (K), and BET surface area distribution (L) of PEI-LNS-2 regeneration after 1 cycle.

theory (Figure 7). Nitrogen isotherms were collected at 77.35 K over a relative pressure range of 0.005−0.995 P/P_0 with a 60 s equilibration time. All LNSs displayed Type II isotherm character with no hysteresis loop present. The linear range of the BET equation was determined using the micropore assistant, included with the Quantachrome TouchWin software package. Five data points were selected between 0.05 and 0.26 P/P_0 to determine the specific surface area for each nanosphere condition. The specific surface area of unmodified LNS was found to be 17.883 m^2 /g. After grafting, the surface area of the PEI-LNS decreased to 13.282 m^2/g. The decrease in surface area is attributed to the blockage of pores in the unmodified LNS. Following SBSS loading, the surface area further decreases to 12.290 m^2/g due to the presence of adsorbed dye molecules on the surface of the nanospheres. Regenerated PEI-LNS-2 demonstrates a higher surface area than the pristine PEI-LNS, but lower than that of the unmodified LNS (14.945 m^2/g). The slight increase in surface area may be explained by the successful removal of SBSS and may indicate the partial removal of grafted amines or surface contaminants previously obstructing access to pore space.

Pore size distributions are calculated using DFT theory using the highest data point on the adsorption isotherm, where all pores are assumed to be saturated with adsorbate. The pore

https://doi.org/10.1021/acsomega.3c09834
ACS Omega 2024, 9, 12006−12014

size distribution of unmodified LNS suggests heterogeneous pores of varying size typically in the mesoporous range of around 8 nm. After grafting with PEI, pore size distribution shifts toward smaller micropores of 1.5 nm, suggesting the filling or partial blockage of pores with the introduced amine. Following the adsorption of SBSS the pore size distribution decreases slightly to 1.4 nm. Removal of SBSS with NaOH for regeneration of the LNS increases the pore size to 1.6 nm, consistent with the increase in the increase in specific surface area due to the partial restoration of some porosity due to the removal of dye and surface contaminants. The TGA shows that the materials are stable at elevated temperatures, with a similar behavior of both LNS and PEI-LNS, showing the feasibility of the material for industrial applications (Figure S7, Supporting Information).

3.3. Adsorption Studies. *3.3.1. Fluorescence Microscopy Imaging.* The SBSS intrinsic fluorescence was leveraged to image the adsorption of the dye by PEI-LNS via fluorescence microscopy. Figure 8 illustrates a comparison of LNS and PEI-LNS-2 upon incubation with the SBSS dye, delineating the ability of PEI-LNS to adsorb dye adsorption.

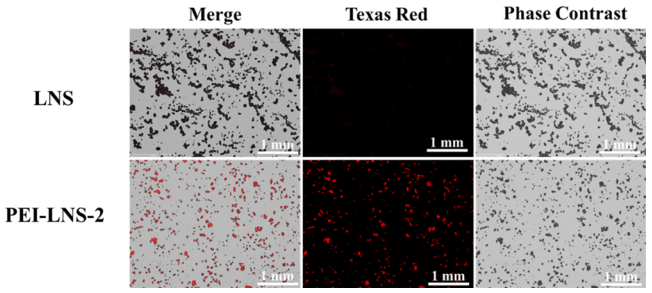

Figure 8. Fluorescence microscopy images of LNS and PEI-LNS-2 exposed to SBSS using an EVOS fluorometer with a Texas Red Light Cube (585/29 nm excitation; 628/32 nm emission).

3.3.2. Effect of pH on Dye Adsorption. To further confirm that electrostatic interactions are a key mechanism of adsorptive removal of SBSS in aqueous solutions, the effect of initial pH on the dye adsorption efficiency and zeta potential of PEI-LNS-2 was evaluated within the pH range of 2.2−8.0 (Figure 9). As expected, high pH values resulted in a decrease in the adsorption capability of PEI-LNS-2, due to deprotonation of the amine groups in PEI at pH values above 6,

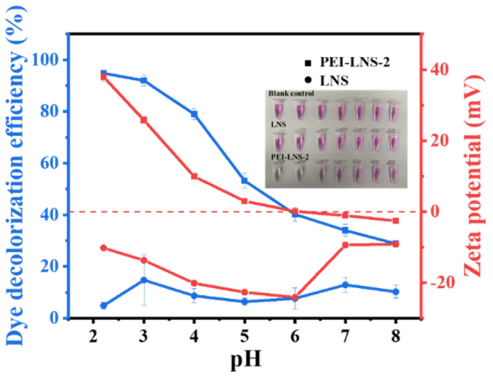

Figure 9. Effect of pH on the zeta potential and adsorptivity of LNS and PEI-LNS-2 toward SBSS (the inset shows the vials with dye solution treated with PEI-LNS-2 and LNS (control), respectively.

consistent with the zeta potential values switching into positive. To explore the maximum adsorption potential of the PEI-LNS, the pH corresponding to the highest zeta potential was selected for further investigations (pH = 2.2).

3.3.3. Nanosorbent Concentration. The concentration of PEI-LNS-2 varied from 0.04 to 0.45 mg/mL. As shown in Figure 10, the dye adsorption efficiency of PEI-LNS-2

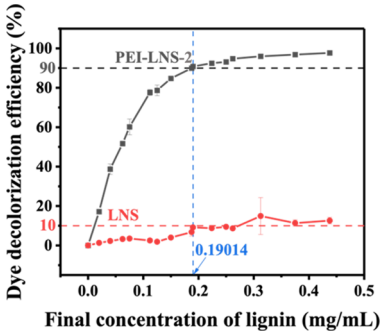

Figure 10. Sorbent dose in relation to the decolorization efficiency of LNS and PEI-LNS-2.

(measured as decolorization of the dye solution) increases noticeably with the concentration of the lignin. At PEI-LNS-2 concentration of 0.19 mg/mL, a 90% adsorption is observed. The adsorption reaches maximum (~100%) at PEI-LNS-2 values above 0.3 mg/mL.

3.3.4. Adsorption Isotherm. The Langmuir (eqs 1−3) and Freundlich (eqs 4 and 5) models were used to study the adsorption isotherms of SBSS in the pH 2.2 adsorbing conditions (equations below):

$$Q_e = \frac{(C_0 - C_e)v}{m} \quad (1)$$

$$Q_e = \frac{K_L \times Q_m \times C_e}{1 + K_L \times C_e} \quad (2)$$

$$\frac{C_e}{Q_e} = \frac{C_e}{Q_m} + \frac{1}{Q_m \times K_L} \quad (3)$$

$$Q_e = K_F C_e \frac{1}{n} \quad (4)$$

$$\log Q_e = \log K_F + \frac{1}{n}\log C_e \quad (5)$$

where C_0 (mg/g) is the initial concentration of the dye, C_e (mg/L) is the equilibrium concentration of the dye, v (L) is the system volume, m (g) is the mass of the adsorbent, Q_e (mg/g) is the maximum adsorption capacity, Q_m (mg/g) is the maximum adsorption capacity of the Langmuir model, K_L (mL/mg) is the Langmuir adsorption coefficient, K_F (mL/mg) is the Freundlich constant, and $\frac{1}{n}$ is an indicator that reflects the nonlinear degree of adsorption.

Both Langmuir and Freundlich adsorption isotherms are shown in Figure 11D. The linear analyses (E and F) indicate that the dye adsorption data for aminated PEI-LNS-2 are in agreement with the Langmuir isotherm model as confirmed by the higher coefficient R^2 (0.999). The Langmuir isotherm analysis indicated that the maximum adsorption capacities of the aminated PEI-LNS-2 is 143.88 mg/g for SBSS dye, which

https://doi.org/10.1021/acsomega.3c09834
ACS Omega 2024, 9, 12006−12014

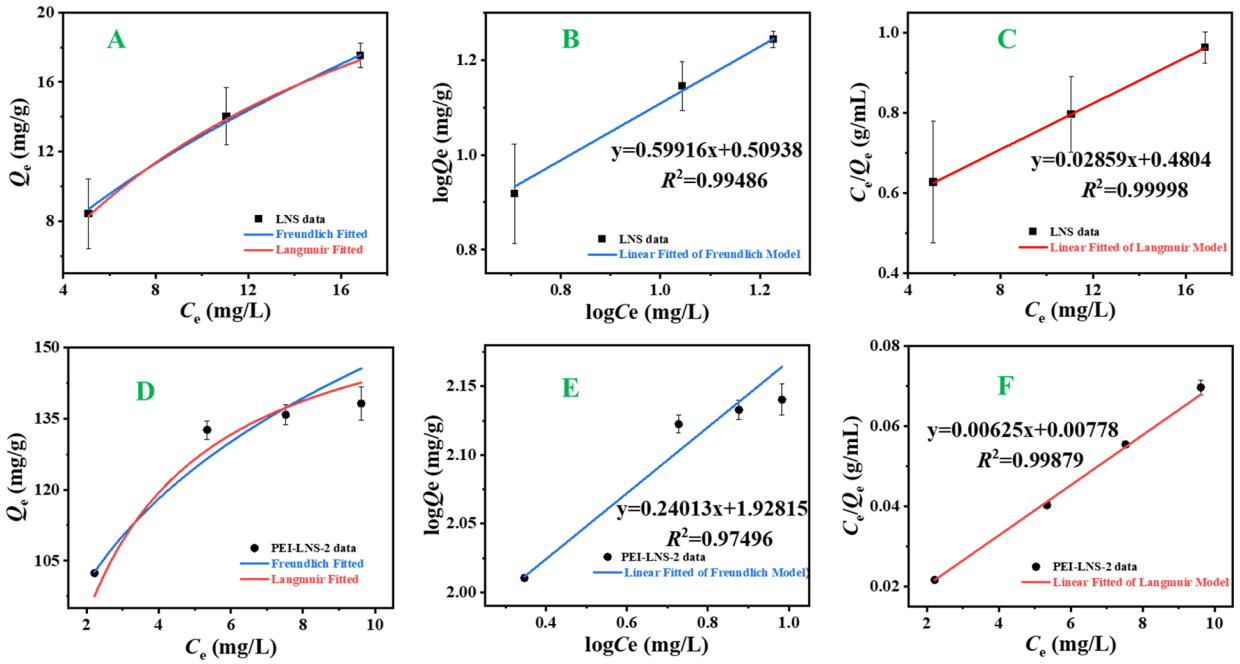

Figure 11. Adsorption isotherms of SBSS by LNS and PEI-LNS-2. (A) Langmuir and Freundlich fitted adsorption isotherm curves of LNS; (B) linear fit of the Freundlich model of LNS (R^2 = 0.995); (C) linear fit of the Langmuir model of LNS (R^2 = 0.999); (D) Langmuir and Freundlich fitted adsorption isotherm curves of PEI-LNS-2; (E) linear fit of the Freundlich model of PEI-LNS-2 (R^2 = 0.975), and (F) linear fit of the Langmuir model of PEI-LNS-2 (R^2 = 0.999).

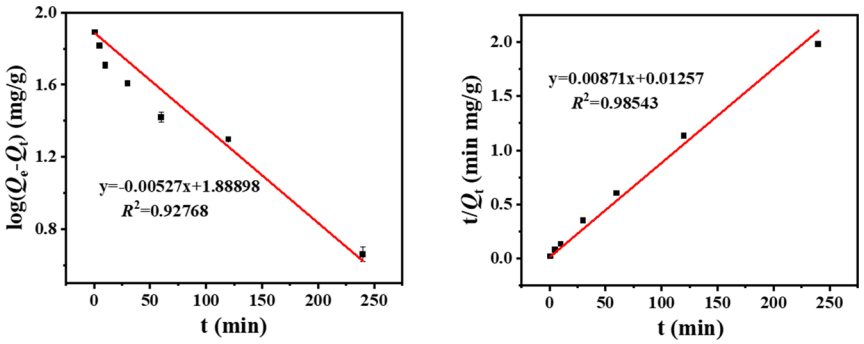

Figure 12. Kinetic models of the adsorption process: pseudo-first-order (left) and pseudo-second-order (right).

Table 2. Parameters of the Adsorption Kinetic Model

kinetic model	equation of linear fit of the model	R^2	Q_e (mg/g)	K_1 (min^{-1}) or K_2 (g mg^{-1} min^{-1})
pseudo-first-order	$y = -0.00527x + 1.88898$	0.92768	77.44	0.012
pseudo-second-order	$y = 0.00871x + 0.01257$	0.98543	114.81	0.006

is unique in the literature for Sulforhodamine dyes and at the forefront of adsorbing capacity when compared with other anionic dyes sorbents.[27]

3.4. Impact of Adsorption Rate. The rate of adsorption is critical in determining the industrial scalability of the process. We input the adsorption process time study data in kinetic models, to identify the adsorption behavior as pseudo-first-order (eq 6) or pseudo-second-order (eq 7):

$$\log(Q_e - Q_t) = \log Q_e - \frac{K_1 t}{2.303} \quad (6)$$

$$\frac{t}{Q_t} = \frac{1}{K_2 Q_e^{\,2}} + \frac{t}{Q_e} \quad (7)$$

where Q_e and Q_t are adsorption capacity (mg/g) at equilibrium time and any instant of adsorption time t (min), and K_1 and K_2 are the rate constant of the pseudo-first-order and second-order adsorption, respectively.

The time study of the adsorption process (Figure S6) suggested that the amount of dye adsorbed increases rapidly in the first 60 min and then the adsorption becomes slow for 8 h until the adsorption equilibrium is reached. The plots in Figure 12 show that the adsorption process is consistent with pseudo-second-order kinetic given the larger value of R^2 (0.985) (Table 2).

3.5. Effect of Ionic Strength. The ionic strength of other contaminants or salts present in wastewater streams can contribute to enhancing or diminishing the adsorbate affinity for the adsorbent due to competition for binding sites;

https://doi.org/10.1021/acsomega.3c09834
ACS Omega 2024, 9, 12006−12014

therefore, this parameter needs to be considered in the evaluation of sorbents for industrial applications. In a typical experiment, the various final concentrations of NaCl were 0, 5, 10, 20, 40, 60, 80, and 100 mM (as showed in Figure 13) and

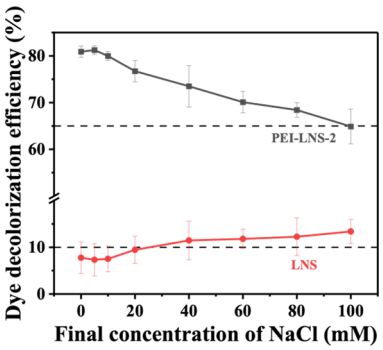

Figure 13. Effect of Salinity on adsorption of SBSS at the LNS and PEI-LNS-2.

the concentrations of the adsorbent (0.15 mg/mL) and SBSS (0.4 mM) were fixed at to explore the effect of ionic strength on SBSS adsorption. Figure 13 depicts the adsorption capacity of PEI-LSN as a function of Na^+ and Cl^- ions concentration. While the dye decolorization efficiency was 80% before the addition of NaCl, it dropped to 65% in the presence of a 100 mM NaCl final solution (an 18.75% decrease), possibly due to a competing effect from the Cl^- ions.

3.6. Regeneration of PEI-LNS-2. Reusability of the adsorbent represents an important aspect to minimize the cost of the overall adsorption process. Regeneration of PEI-LNS-2 followed by reuse was performed for four cycles (Figure 14), as follows. After the adsorption step, the PEI-LNS-2

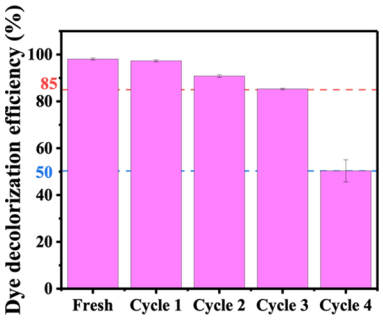

Figure 14. Dye decolorization efficiency of PEI-LNS-2 for SBSS dye after four adsorption−desorption cycles.

material was collected by centrifugation, and 100 μL of 0.1 mM NaOH solution was added to the tube to promote amine deprotonation and hence drive electrostatic repulsion of the anionic dye. The dispersion was allowed to shake for 4 h, and the PEI-LNS-2 was collected again by centrifugation, dried overnight in a vacuum oven at room temperature, and reused the next day in a new adsorption step. The adsorption efficiency decreased gradually within 3 adsorption−desorption cycles (to 98, 90, and 85% after each subsequent cycle), dropping to around 50% in the fourth cycle. This demonstrates that PEI-LNS-2 could be a feasible, inexpensive, and environmentally friendly sorbent.

4. CONCLUSIONS

Research on inexpensive biobased adsorbents for the removal of harmful substances from effluents has recently attracted significant attention. In this study, a new platform for anionic contaminants removal was prepared and tested. The TMS-LNSs PEI-LNS-2 were prepared from LNSs using a PEI-functionalized silane linker. This is the first report of an amine-modified LNS developed for the environmental remediation of anionic substances. The adsorption capacity of this novel sorbent toward removing an anionic dye (SBSS) from water was demonstrated under various conditions, including simulated salinity and pH of industrial waste streams. Kinetics studies demonstrated that SBSS adsorption using PEI-LNS-2 follows pseudo-second-order kinetics. The Langmuir isotherm model was used to fit the adsorption profile, enabling the determination of a maximum adsorption capacity Q_m of 143.88 mg/g, at pH 2.2. The sorbent could be regenerated by treatment with NaOH, which renders a maximum of 85% adsorption efficiency after 3 cycles. The study demonstrated that the novel nanomaterial, consisting of polyamine-functionalized LNSs, is a promising candidate for the environmental cleanup of anionic dyes from wastewater effluents.

■ ASSOCIATED CONTENT

Supporting Information

The Supporting Information is available free of charge at https://pubs.acs.org/doi/10.1021/acsomega.3c09834.

STEM EDX map of PEI-LNS-2, FE-SEM images of PEI-LNS-1/3/4, ^{1}H NMR spectra of LNS and PEI-LNS in DMSO, ^{13}C NMR solid-state NMR spectra of LNS and PEI-LNS, UV−vis spectrum of SBSS and a calibration curve of SBSS, effect time on dye adsorption efficiency; TGA of dried raw lignin, LNS and PEI-LNS-2, concentrations of the lignin adsorbent utilized; photographs and SEM images pre- and post- adsorption; FT-IR of the PEI-LNS post-SBSS adsorption and SBSS; and selectivity of the sorbent for anionic dyes (PDF)

■ AUTHOR INFORMATION

Corresponding Author

Cheng-Yu Lai − *Department of Mechanical and Materials Engineering and Department of Chemistry and Biochemistry, Florida International University, Miami, Florida 33174, United States;* orcid.org/0000-0002-8931-5601; Email: clai@fiu.edu

Authors

Fei Zhang − *Department of Mechanical and Materials Engineering, Florida International University, Miami, Florida 33174, United States*

Ha Na − *Department of Mechanical and Materials Engineering, Florida International University, Miami, Florida 33174, United States;* orcid.org/0000-0003-0872-7231

Jake Carrier − *Department of Chemistry and Biochemistry, Florida International University, Miami, Florida 33174, United States*

Chen-Yu Chang − *Department of Mechanical and Materials Engineering, Florida International University, Miami, Florida 33174, United States;* orcid.org/0000-0001-5253-1813

Daniela Radu − *Department of Mechanical and Materials Engineering, Florida International University, Miami, Florida 33174, United States;* orcid.org/0000-0001-6833-5825

https://doi.org/10.1021/acsomega.3c09834
ACS Omega 2024, 9, 12006−12014

Complete contact information is available at:
https://pubs.acs.org/10.1021/acsomega.3c09834

Author Contributions

The manuscript was written through the contributions of all authors. All authors have given approval to the final version of the manuscript.

Notes

The authors declare no competing financial interest.

■ ACKNOWLEDGMENTS

This work was supported by USDA-NIFA, Award # 2021-67022-33468, and in part by the NSF, Award # DMR-2122078, and NASA Award # 80NSSC19M0201. The authors thank Mr. Bharavi Misra and Dr. Joshua Stapleton at Pennsylvania State University for STEM access, and Ms. Christy George at Penn State for the NMR spectroscopy. Jake Carrier acknowledges the support from an FIU Veteran Fellowship awarded by the FIU Graduate School.

■ REFERENCES

(1) Shin, J.-H.; Yang, J. E.; Park, J. E.; Jeong, S.-W.; Choi, S.-J.; Choi, Y. J.; Jeon, J. Rapid and Efficient Removal of Anionic Dye in Water Using a Chitosan-Coated Iron Oxide-Immobilized Polyvinylidene Fluoride Membrane. *ACS Omega* **2022**, *7* (10), 8759−8766.
(2) Berradi, M.; Hsissou, R.; Khudhair, M.; Assouag, M.; Cherkaoui, O.; El Bachiri, A.; El Harfi, A. Textile finishing dyes and their impact on aquatic environs. *Heliyon* **2019**, *5* (11), No. e02711.
(3) De Jesús-González, A.; Rangel-Vázquez, N.-A.; De Velasco-Maldonado, P.-S. Chapter 19 - Thermodynamic and structural analysis of graphene/polymer nanocomposites for the adsorption of azo dyes present in binary mixed. In *Novel Materials for Environmental Remediation Applications*, Giannakoudakis, D. A., Meili, L., Anastopoulos, I., Eds.; Elsevier, 2023; 509−535.
(4) Mittal, A.; Mittal, J.; Malviya, A.; Kaur, D.; Gupta, V. K. Adsorption of hazardous dye crystal violet from wastewater by waste materials. *J. Colloid Interface Sci.* **2010**, *343* (2), 463−473.
(5) Fang, Y.; Zhao, G.; Dai, W.; Ma, L.; Ma, N. Enhanced adsorption of rubidium ion by a phenol@MIL-101(Cr) composite material. *Microporous Mesoporous Mater.* **2017**, *251*, 51−57.
(6) Awad, A. M.; Jalab, R.; Benamor, A.; Nasser, M. S.; Ba-Abbad, M. M.; El-Naas, M.; Mohammad, A. W. Adsorption of organic pollutants by nanomaterial-based adsorbents: An overview. *J. Mol. Liq.* **2020**, *301*, No. 112335.
(7) Wang, T.; Jiang, M.; Yu, X.; Niu, N.; Chen, L. Application of lignin adsorbent in wastewater Treatment: A review. *Sep. Purif. Technol.* **2022**, *302*, No. 122116.
(8) Bajwa, D. S.; Pourhashem, G.; Ullah, A. H.; Bajwa, S. G. A concise review of current lignin production, applications, products and their environmental impact. *Industrial Crops and Products* **2019**, *139*, No. 111526.
(9) Ragauskas, A. J.; Beckham, G. T.; Biddy, M. J.; Chandra, R.; Chen, F.; Davis, M. F.; Davison, B. H.; Dixon, R. A.; Gilna, P.; Keller, M.; et al. Lignin valorization: improving lignin processing in the biorefinery. *Science* **2014**, *344* (6185), No. 1246843.
(10) Mun, S. P.; Cai, Z.; Zhang, J. Fe-catalyzed thermal conversion of sodium lignosulfonate to graphene. *Mater. Lett.* **2013**, *100*, 180−183.
(11) Delmas, M. Vegetal Refining and Agrochemistry. *Chem. Eng. Technol.* **2008**, *31* (5), 792−797.
(12) Patil, P. T.; Armbruster, U.; Richter, M.; Martin, A. Heterogeneously Catalyzed Hydroprocessing of Organosolv Lignin in Sub- and Supercritical Solvents. *Energy Fuels* **2011**, *25* (10), 4713−4722.
(13) Gosselink, R. J.; Teunissen, W.; van Dam, J. E.; de Jong, E.; Gellerstedt, G.; Scott, E. L.; Sanders, J. P. Lignin depolymerisation in supercritical carbon dioxide/acetone/water fluid for the production of aromatic chemicals. *Bioresour. Technol.* **2012**, *106*, 173−177.
(14) Zakzeski, J.; Bruijnincx, P. C. A.; Jongerius, A. L.; Weckhuysen, B. M. The Catalytic Valorization of Lignin for the Production of Renewable Chemicals. *Chem. Rev.* **2010**, *110* (6), 3552−3599.
(15) Haveren, J. V. Bulk chemicals from biomass. *Biofuels Bioprod. Biorefining* **2008**, *2* (1), 41−57.
(16) SjöströM, E. Chapter 4 - LIGNIN. In *Wood Chemistry*, (Second ed.); Academic Press, 1993; 71−89.
(17) Supanchaiyamat, N.; Jetsrisuparb, K.; Knijnenburg, J. T. N.; Tsang, D. C. W.; Hunt, A. J. Lignin materials for adsorption: Current trend, perspectives and opportunities. *Bioresour. Technol.* **2019**, *272*, 570−581.
(18) Upton, B. M.; Kasko, A. M. Strategies for the Conversion of Lignin to High-Value Polymeric Materials: Review and Perspective. *Chem. Rev.* **2016**, *116* (4), 2275−2306.
(19) Salih, S. J.; Abdul Kareem, A. S.; Anwer, S. S. Adsorption of anionic dyes from textile wastewater utilizing raw corncob. *Heliyon* **2022**, *8* (8), No. e10092.
(20) Österberg, M.; Sipponen, M. H.; Mattos, B. D.; Rojas, O. J. Spherical lignin particles: a review on their sustainability and applications. *Green Chem.* **2020**, *22* (9), 2712−2733.
(21) Qian, Y.; Deng, Y.; Qiu, X.; Li, H.; Yang, D. Formation of uniform colloidal spheres from lignin, a renewable resource recovered from pulping spent liquor. *Green Chem.* **2014**, *16* (4), 2156.
(22) Zhang, L.; Zhou, Y.; Jin, X.; Du, X.; Li, B. The microstructure and high-temperature properties of novel nano precipitation-hardened face centered cubic high-entropy superalloys. *Scripta Materialia* **2018**, *146*, 226−230.
(23) Molavi, H.; Salimi, M. S. Green Synthesis of Cerium-Based Metal−Organic Framework (Ce-UiO-66 MOF) for Wastewater Treatment. *Langmuir* **2023**, *39* (49), 17798−17807.
(24) Satilmis, B.; Budd, P. M. Selective dye adsorption by chemically-modified and thermally-treated polymers of intrinsic microporosity. *J. Colloid Interface Sci.* **2017**, *492*, 81−91.
(25) An, L.; Si, C.; Bae, J. H.; Jeong, H.; Kim, Y. S. One-step silanization and amination of lignin and its adsorption of Congo red and Cu(II) ions in aqueous solution. *Int. J. Biol. Macromol.* **2020**, *159*, 222−230.
(26) Boeriu, C. G.; Bravo, D.; Gosselink, R. J. A.; van Dam, J. E. G. Characterisation of structure-dependent functional properties of lignin with infrared spectroscopy. *Industrial Crops and Products* **2004**, *20* (2), 205−218.
(27) Meng, X.; Scheidemantle, B.; Li, M.; Wang, Y.-y.; Zhao, X.; Toro-González, M.; Singh, P.; Pu, Y.; Wyman, C. E.; Ozcan, S.; et al. Synthesis, Characterization, and Utilization of a Lignin-Based Adsorbent for Effective Removal of Azo Dye from Aqueous Solution. *ACS Omega* **2020**, *5* (6), 2865−2877.